

Synchronization in Networks of Heterogeneous Kuramoto–Sakaguchi Oscillators with Higher-order Interactions

Asutosh Anand Singh ¹ and Chandrakala Meena ¹

¹ Physics Department, Indian Institute of Science Education and Research (IISER), Pune, 411008, Maharashtra, India.

(Dated: December 12, 2025)

How do the combined effects of phase frustration, noise, and higher-order interactions govern synchronization in globally coupled heterogeneous Kuramoto oscillators? To address this question, we investigate a globally coupled network of Kuramoto–Sakaguchi oscillators that includes both pairwise ($1 - \text{simplex}$) and higher-order ($2 - \text{simplex}$) interactions, together with additive stochastic forcing. Systematic numerical simulations across a broad range of coupling strengths, phase-lag values, and noise intensities reveal that synchronization emerges through a nontrivial interplay among these parameters. In general, weak frustration combined with mutually reinforcing coupling promotes synchronization, whereas strong frustration favors coherence under repulsive coupling. Increasing noise progressively suppresses coherence, smoothening the transition from desynchronized to synchronized states. Forward and backward parameter sweeps reveal the coexistence of synchronized and desynchronized states. The presence and width of this bistable region depend sensitively on phase frustration, noise intensity, and higher-order coupling strength, with higher-order interactions significantly widening the bistable interval. To explain these behaviors, we employ the Ott–Antonsen reduction to derive a low-dimensional amplitude equation that predicts the forward critical point in the thermodynamic limit, the backward saddle-node point, and the width of the bistable region. Higher-order interactions widen this region by shifting the saddle-node point without affecting the forward critical point. Further analysis of Kramer’s escape rate explains how noise destabilizes co-existence states and diminishes bistability. Overall, our results provide a unified theoretical and numerical framework for frustrated, noisy, higher-order oscillator networks, revealing that synchronization is strongly influenced by the combined action of phase frustration, stochasticity, and both pairwise and higher-order interactions.

I. INTRODUCTION

The emergence of synchronization in large networks of coupled oscillators stands as a central theme in nonlinear dynamics and complex systems, with wide-ranging applications in physics, neuroscience, engineering, and the social sciences [1–4]. The term "synchronization" derives from the Greek words "syn" (meaning "together") and "chronos" (meaning "time") [5], reflecting the alignment of oscillatory rhythms, either among interacting components or with an external driving force.

Synchronization has been recognized as a ubiquitous phenomenon across both natural and engineered systems, encompassing areas such as biological populations [2] and systems [6, 7], climate [8], power grids, and communication networks [9]. Depending upon system properties and couplings, synchronization can manifest in various forms, including phase [10, 11], frequency [12], and amplitude synchronization [13, 14]. A major milestone in the study of collective synchronization was achieved with the introduction of the Kuramoto model, which describes a population of globally coupled phase oscillators interacting through sinusoidal functions of their phase differences [15, 16]. Despite its apparent simplicity, the Kuramoto model captures a nonequilibrium phase transition from incoherence to collective synchrony when the coupling strength exceeds a critical threshold [17, 18]. Since then, this framework has been widely applied across diverse domains, including Josephson junction arrays [19, 20], ensembles of neurons [21, 22], and firefly flashing [2], cricket chirping [23]. In the social sciences, Kuramoto-type models have been used to study crowd synchronization, such as people walking on

bridges [24, 25].

The low-dimensional reduction method introduced by Ott and Antonsen [26] further enabled an elegant analytical study of such high-dimensional oscillator ensembles, making the Kuramoto framework a foundational model for understanding emergent synchronization in complex systems.

The Kuramoto model has been extended to incorporate more realistic features, such as nontrivial frequency distributions [27, 28], heterogeneous network topologies [29], and higher harmonics [30]. Recent studies have highlighted that pairwise network dynamical frameworks are often insufficient, as many real systems involving simultaneous multi-body interactions are modeled using simplicial complexes and hypergraphs [31, 32]. This approach also leads to the definition of a useful global synchronization measure known as the Kuramoto–Daido order parameter [30]. Incorporating such higher-order interactions has revealed abrupt synchronization transitions [33], and multistability [34].

A significant factor influencing the collective dynamics of coupled Kuramoto oscillators is frustration [35], typically introduced through a phase lag in the coupling function as described by the sine term in the Sakaguchi–Kuramoto (SK) oscillators ensemble. Coupled SK oscillators exhibit behaviors such as the coexistence of synchronized and desynchronized states known as chimera, in which coherent and incoherent oscillator groups emerge simultaneously, and partially synchronized states that interpolate between full order and complete incoherence [27, 36].

Stochasticity is also unavoidable in engineered systems such as [37, 38], arising from intrinsic variability or ex-

ternal disturbances. Noise can destabilize coherence by inducing random phase slips or, under certain circumstances, favor synchronization through noise-induced ordering. The net effect depends sensitively on the noise intensity and the underlying coupling structure of the system [39].

Over the past several decades, numerous studies have investigated the separate roles of phase frustration, stochasticity[40], and higher-order interactions in shaping synchronization. Yet their joint impact, especially in systems with explicit multi-body coupling terms, remains poorly understood. A unified framework that simultaneously accounts for phase frustration, noise, and higher-order coupling is still missing but has been explored in the case of pairwise coupling [41].

In this work, we address this gap by investigating a globally coupled network of Kuramoto–Sakaguchi oscillators augmented with both pairwise ($1 - \text{simplex}$) and higher-order ($2 - \text{simplex}$) interactions under stochastic forcing. Through numerical simulations and the Ott–Antonsen (OA) reduction, we demonstrate how the interplay between phase frustration, noise, and higher-order coupling profoundly affects synchronization. Our results demonstrate that higher-order interactions can accelerate the onset of synchronization, expand the bistable region, and mitigate the desynchronization effects of frustration and noise. We analyze the resulting multistability using the reduced amplitude equation and further quantify the stability of metastable states using Kramer’s escape theory, which explains how noise modulates hysteresis width. Overall, this study presents a unified theoretical and computational framework for synchronization in oscillator networks, where the combined effects of frustration, stochasticity, and higher-order interactions are crucial for modeling the real-world complex systems.

Our paper is organized as follows: Section II introduces the dynamical framework and presents the numerical results obtained from simulations. Section III provides the analytical results derived via the Ott–Antonsen reduction, followed by fixed-point analysis, stability characterization, bifurcation diagrams, and multistable states analysis using Kramer’s escape rate. Finally, Section IV summarizes and discusses the main findings of the study.

II. MODEL DESCRIPTION AND NUMERICAL SIMULATIONS

In our study, we consider the Sakaguchi-Kuramoto (SK) model [42], which is an extension of the Kuramoto model [18] through the inclusion of a phase lag term (*frustration*) in the coupling function. We focus on a globally (all-to-all) coupled phase-oscillator system (see Fig.1a), considering $2 - \text{simplex}$ interactions along with $1 - \text{simplex}$ interactions represented using various colors (see Fig.1b). The dynamical

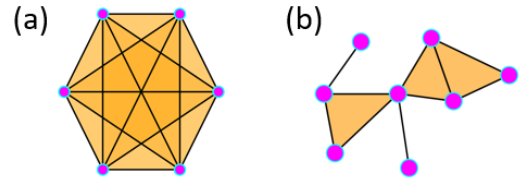


FIG. 1. A representative architecture of the globally coupled oscillator system where the nodes ($0 - \text{simplexes}$) are represented by magenta color, the pairwise connections, that is, the edges ($1 - \text{simplexes}$), are represented by black lines, and higher-order interactions ($2 - \text{simplexes}$, filled triangles) are represented by orange color. Panel (a) represents all-to-all coupling, whereas panel (b) represents a smaller version of simplices.

ical equation for each oscillator in the network is given by:

$$\begin{aligned} \dot{\theta}_i = & \omega_i + \frac{k_1}{N} \sum_{j=1}^N \sin(\theta_j - \theta_i - \beta) \\ & + \frac{k_2}{N^2} \sum_{j=1}^N \sum_{l=1}^N \sin(2\theta_j - \theta_l - \theta_i - \beta) + \zeta_i(t), \end{aligned} \quad (1)$$

Here, ω_i and θ_i denote the intrinsic natural frequency and phase of the oscillator, i ($i = 1, 2, \dots, N$). Here, N is the total number of oscillators or nodes in the network, and β is the phase-lag parameter that introduces *frustration* into the system. We consider nonidentical oscillators by taking distinct natural frequencies ω_i for each node, drawn from the Lorentzian distribution[43], $g(\omega) = \frac{\Delta}{\pi[(\omega - \omega_0)^2 + \Delta^2]}$, where ω_0 is the mean frequency and Δ is the width of the distribution. Throughout this study, we analyze the nonzero-frequency case, i.e., $\omega_i \neq 0$. The second term in Eq. 1 corresponds to pairwise ($1 - \text{simplex}$) interactions with coupling strength k_1 , while the third term accounts for higher-order ($2 - \text{simplex}$) interactions with coupling strength k_2 . The last term introduces stochasticity in the system, where $\zeta_i(t)$ represents Gaussian white noise with zero mean, δ correlated in time, and independent across oscillators. Specifically, $\langle \zeta_i(t) \rangle = 0$ and $\langle \zeta_i(t) \zeta_j(t') \rangle = 2D \delta_{ij} \delta(t - t')$, where $D \geq 0$ denotes the noise strength.

In the Kuramoto framework, the degree of synchronization is quantified by the magnitude r of the complex order parameter z . It is often referred to as the order parameter, and it takes values in the range $0 \leq r \leq 1$. The general expression for z is given by [44]:

$$z_m(t) = r e^{im\psi_m} = \frac{1}{N} \sum_{j=1}^N e^{im\theta_j} \quad (2)$$

where m represents the order of interactions; this implies $m = 1$ for $1 - \text{simplex}$ and $m = 2$ for $2 - \text{simplex}$ interactions, respectively. Similarly, ψ_m denotes the mean phase, while θ_j represents the phase of the j -th oscillator. The order-parameter equation for the pairwise interactions is written

as;

$$z_1(t) = r_1 e^{i\psi_1} = \frac{1}{N} \sum_{j=1}^N e^{i\theta_j} \quad (3)$$

where $r_1 = |z_1|$ is the amplitude of the order-parameter z_1 .

Similarly, by setting $m = 2$ in the general order parameter definition (Eq. 2), one obtains a higher-order order parameter that quantifies the degree of synchronization due to triadic (2-simplex) interactions in the system, given by

$$z_2(t) = r_2 e^{2i\psi_2} = \frac{1}{N} \sum_{j=1}^N e^{i2\theta_j} \quad (4)$$

where $r_2 = |z_2|$ is the amplitude of the complex order-parameter z_2 .

Throughout this paper, we take $R (= r_1)$ as a measure of the system's synchronization. The case $R = 0$ corresponds to a completely desynchronized state, where all oscillators are uniformly spread around the unit circle, whereas $R = 1$ indicates a fully synchronized state with all oscillators perfectly phase-aligned (a one-cluster state).

The study begins with a numerical investigation of the synchronization dynamics of a globally coupled network of nonidentical SK oscillators, modeled by Eq. 1 with a network of size $N = 100$. The initial conditions for the system are an equally populated bicluster state with 50 oscillators having phase $\phi = 0$, and the remaining oscillators have phase $\phi = \pi$. The intrinsic frequencies ω of the oscillators are drawn from a Lorentzian frequency distribution with a mean frequency $\omega_0 = 0$ and width $\Delta = 0.5$. To find the influence of stochasticity on the system's behavior, three distinct noise strengths are considered: $D = 0.0, 0.5, 1.0$.

Synchronization in the (k_1, β) Space: To analyze the emergence of synchronization in the coupled system modeled by Eq. 1, we first examine the order parameter in the (k_1, β) parameter space. Specifically, k_1 and β are varied within the ranges $k_1 \in [-15, 15]$ and $\beta \in [-\pi, \pi]$, respectively. For each fixed value of k_2 , we investigate synchronization among oscillators for three representative noise strengths: $D = 0.0, 0.5$, and 1.0 by calculating the order parameter R . Since the range of 1-simplex interaction strength $k_1 \in [-15, 15]$, we choose five distinct values of 2-simplex interaction strength, $k_2 = -20, -10, 0, 10$ and 20 , thereby covering the transition from strongly repulsive to strongly attractive triadic interactions in the network.

Figure 2 illustrates the dynamical regions in the (k_1, β) parameter space, and several salient trends can be identified that influence the emergence of synchronization within the network. For example, for the noiseless case ($D = 0$), as shown in Figs. 2(a,d,g,j,m), the network exhibits synchronized and desynchronized regimes in (k_1, β) space, and the extent of these regions strongly depends on the 2-simplex strength k_2 . For example, Fig. 2(g), which corresponds to the absence of higher-order interactions ($k_2 = 0$), shows a synchronization region that is symmetrically distributed

around $\beta = 0$. The extent of the synchronized and desynchronized regions in the (k_1, β) space depends on the values of k_2 . Specifically, for $k_1 > 0$, synchronization emerges when $\beta \in (-\pi/2, \pi/2)$, whereas for $k_1 < 0$, synchronization occurs in the regions $\beta \in (\pi/2, \pi]$ and $\beta \in (-\pi/2, -\pi]$. This indicates that positive (mutual) pairwise couplings favor synchronization when the intrinsic phase frustration of the oscillators is relatively small.

At strong negative 2-simplex coupling strength ($k_2 = -20$ cf. Fig. 2(a)), synchronization predominantly appears when the intrinsic phase lag lies within $\beta \in (-\pi/2, -\pi]$ and $\beta \in (\pi/2, \pi]$, and $k_1 \in [-15, 1.5]$. This indicates that for strong repulsive higher-order interactions, synchronization is sustained only when pairwise interactions are repulsive or weakly mutual.

As k_2 decreases to -10 (cf. Fig. 2(d)), synchronized regimes emerge for negative values of k_1 , particularly when the phase lag lies within the ranges $\beta \in (-\pi/2, -\pi]$ and $\beta \in (\pi/2, \pi]$. For large negative values of k_1 , the synchronized regions expand and cover nearly the entire aforementioned β range, compared to the narrower bands observed at less negative k_1 . Additionally, we observe that synchronization gradually begins to appear on the right-hand side of the (k_1, β) plane for larger positive k_1 values with increasing k_2 values. This behavior suggests that weaker repulsive triadic couplings can partially alleviate phase frustration and facilitate the emergence of coherence among oscillators, even when k_1 is positive and large.

For $k_2 > 0$, the synchronization regimes shift markedly in (k_1, β) space; for instance, at $k_2 = 10$ (cf Fig. 2(j)), a distinct synchronized region (red lobe) emerges for $k_1 \in [0, 15]$, and weak synchronization begins to appear even for slightly negative k_1 , reflecting the partial stabilization effect of positive higher-order interactions. This tendency becomes more pronounced at $k_2 = 20$ (cf Fig. 2(m)), where the synchronized region broadens and forms an almost symmetric red domain around $\beta = 0$, extending across $\beta \in (-\pi/2, \pi/2)$. This shift demonstrates that strong positive triadic interactions can effectively counteract the desynchronization influence of phase frustration and weaker pairwise coupling, thereby restoring coherence in the network.

These observations collectively suggest that when the intrinsic phase lag lies within $\beta \in (-\pi/2, \pi/2)$, oscillators either lag behind ($\beta > 0$) or lead ($\beta < 0$) their neighbors, resulting in weak phase frustration among the nodes. To overcome this weak frustration and sustain synchronization, k_1 must be sufficiently large, although its critical value depends sensitively on k_2 . For example, from Fig. 2(m), it is evident that when $k_2 = 20$, synchronization emerges from $k_1 \approx -1.5$, whereas for $k_2 = -10$, synchronization appears only for larger k_1 values near $k_1 \approx 14$ (see Figs. 2(d)).

In contrast, when the intrinsic phase lag lies within $\beta \in (\pm\pi/2, \pm\pi]$, the degree of frustration is stronger, leading to more repulsive coupling among oscillators. In such cases, synchronization can emerge only when k_2 is also repulsive (negative) and k_1 is predominantly negative, although small positive k_1 values may still permit weak coherence for strongly negative k_2 (see Fig. 2(a)). Hence, synchronization

in this region is possible only when the coupling strengths are sufficiently negative to counterbalance the strong intrinsic phase frustration effect on synchronization.

The influence of stochasticity on these patterns is captured in the middle and right columns of Fig. 2, corresponding to $D = 0.5$ and $D = 1.0$, respectively. From Figs. 2(b, e, h, k, n) and Figs. 2(c, f, i, l, o), it is evident that introducing noise progressively diminishes the synchronized regimes across the same (k_1, β) parameter range. We also observe that the transition from desynchronization to synchronization becomes smoother in the presence of noise. This demonstrates that stochastic fluctuations disrupt phase alignment among oscillators, transforming the sharp first-order synchronization transitions observed in the deterministic system into continuous and second-order transitions at higher noise intensities.

Overall, these observations highlight that synchronization in a network of coupled oscillators arises from the intricate interplay among pairwise and triadic interactions, intrinsic phase frustration, and stochastic fluctuations. When intrinsic phase frustration is weak, broadly, synchronization is favored for both positive coupling strengths. However, under strong phase frustration, coherence emerges only when both coupling strengths are repulsive. High levels of stochasticity tend to suppress overall coherence among oscillators and simultaneously smooth the transition from desynchronization to synchronization.

Forward and backward simulations: In the forward simulation, the system is initialized in an equally populated bicluster configuration and evolves while the value of k_1 is gradually increased. Once the system reaches a synchronized state, this final configuration is used as the initial condition for the backward simulation, in which k_1 is decreased in small, gradual steps (refer to Fig. 3 and Fig. 4).

The forward sweep, FS (magenta), and backward sweep, BS (cyan), branches reveal that the coupled system may exhibit hysteresis, and the width of this hysteresis depends on β , D , and k_2 . For example, Figs. 3(a,d,g) show clear hysteresis loops whose widths progressively shrink as the phase lag β increases, for a fixed set of the remaining parameters. Similarly, Figs. 3(a,b,c) illustrate that hysteresis persists only up to a certain level of stochasticity, and the hysteresis width decreases as the noise intensity D increases.

From Fig. 3 and Fig. 4, it is evident that the higher-order interaction strength k_2 plays a major role in widening the multistable region. This behavior differs from the finite-size effect reported in [45], where the system size controls the width of the multistable region.

To understand the mechanism behind the emergence of bistability between synchronized and desynchronized states in our coupled network, we further analyze the system dynamics theoretically, as described in the following sections.

III. LOW-DIMENSIONAL MODEL AND ANALYTICAL RESULTS

Fig. 2 illustrates that the system undergoes different types of transitions from desynchronized to synchronized states, depending on the parameter values. For instance, in Fig. 2(j), when the phase lag β approaches zero, even a small increase in the pairwise coupling strength k_1 near $k_1 = 0$ (in the positive direction) leads to an abrupt jump to synchronization, indicating a first-order transition. In contrast, some transitions occur more smoothly. For example, Fig. 2(f) shows a gradual increase in coherence with increasing k_1 , characteristic of a second-order phase transition. Fig. 3 and Fig. 4 clearly exhibit both first- and second-order transitions, depending on the specific combination of parameters (k_2, β, D) .

To capture such transitions, we simplify the globally coupled oscillators network by utilizing the Ott-Antonsen (OA) approach[26], which reduces the coupled system equation to a lower dimension, irrespective of the system size. The OA method substantially simplifies the problem while preserving the characteristics of the globally coupled system. This technique begins with an assumption that in the continuum limit ($N \rightarrow \infty$), the system is characterized by a density function $\rho(\theta, \Omega, t)$, and its temporal evolution is governed through the Fokker-Planck (continuity) equation.

$$\frac{\partial \rho}{\partial t} = -\frac{\partial(v\rho)}{\partial \theta} + D \frac{\partial^2 \rho}{\partial \theta^2} \quad (5)$$

Here, D denotes the noise strength and v represents velocity, which is defined as (please refer to Sec. 1 of the supplementary material for detailed steps to find v);

$$v(\theta, \omega, t) = \omega_i + \frac{1}{2i} \left(H e^{-i(\theta+\beta)} - H^* e^{i(\theta+\beta)} \right) \quad (6)$$

where, $H = (k_1 z_1 + k_2 z_2 \bar{z}_1)$ and H^* is the complex conjugate of H . The order parameter ($z_m = r_m e^{i\psi_m}$, $m = 1, 2$) in the continuum limit ($N \rightarrow \infty$) can be written as:

$$z_1 = r_1 e^{i\psi_1} = \int_0^{2\pi} \int_{-\infty}^{\infty} \int_{-\infty}^{\infty} e^{i\phi} \rho(\phi, \omega, \Omega, t) g(\Omega) d\Omega d\omega d\phi \quad (7)$$

$$z_2 = r_2 e^{i\psi_2} = \int_0^{2\pi} \int_{-\infty}^{\infty} \int_{-\infty}^{\infty} e^{2i\phi} \rho(\phi, \omega, \Omega, t) g(\Omega) d(\Omega) d(\omega) d(\phi) \quad (8)$$

where z_1 corresponds to the order parameter for pairwise interaction and z_2 represents the order parameter for 2-simplices interactions. The solution of Eq.5, using the Ott-Antonsen ansatz, can be written by expanding the probability density function (ρ), in terms of the Fourier series:

$$\rho(\theta, \Omega, t) = \frac{g(\Omega)}{2\pi} \left(1 + \sum_{n=1}^{\infty} \rho_n(\Omega, t) e^{in\theta} + c.c \right) \quad (9)$$

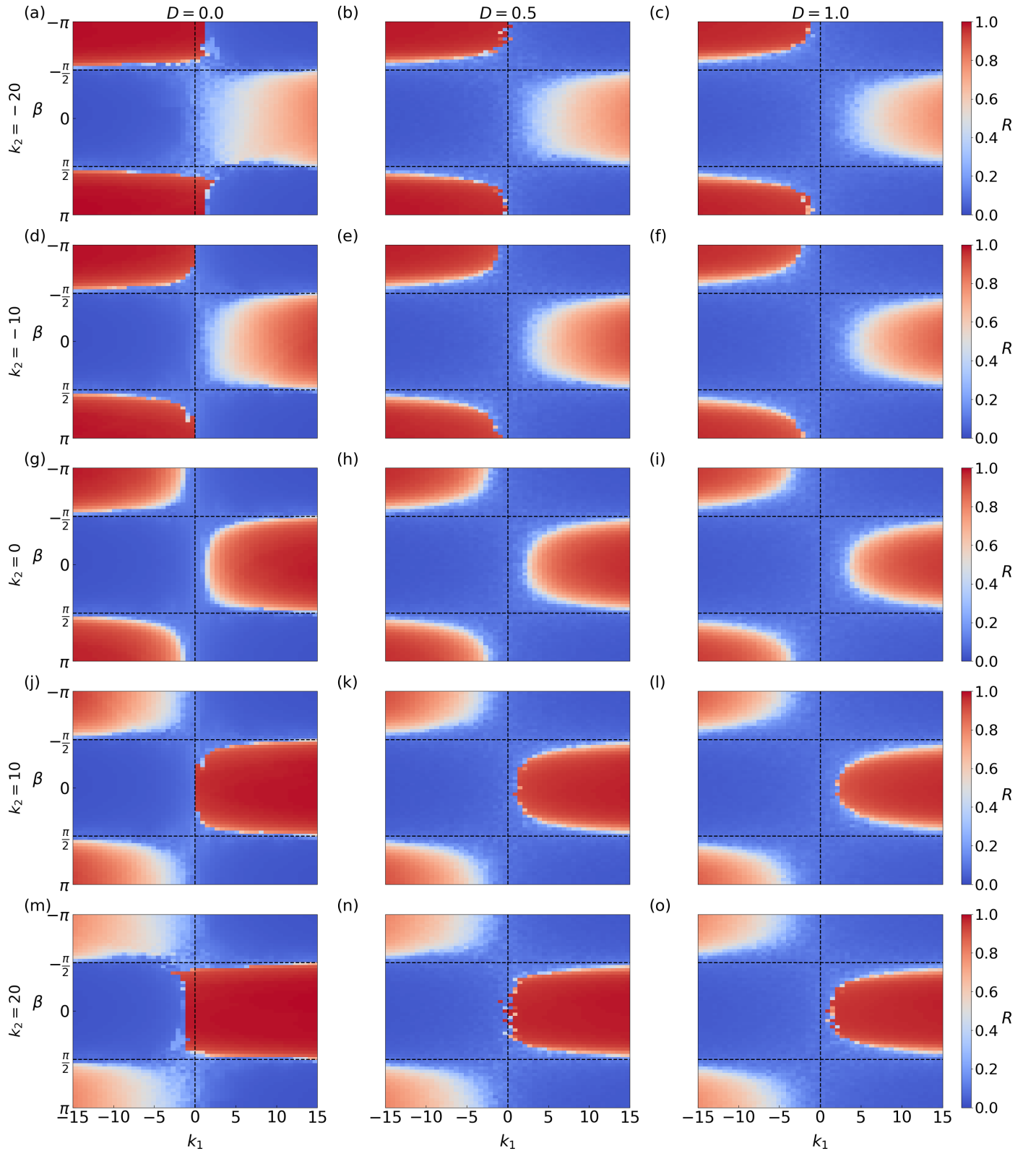


FIG. 2. Synchronization landscapes in the (k_1, β) parameter space for a network of $N = 100$ frustrated stochastic Kuramoto oscillators incorporating higher-order (2-simplex) interactions. The degree of collective coherence is measured by the order parameter R . The color map encodes the value of R , with dark blue ($R = 0$) corresponding to a fully desynchronized state and red ($R = 1$) indicating complete synchronization. Each column represents a distinct noise strength, $D = 0, 0.5$, and 1 , while each row corresponds to a fixed value of the 2-simplex coupling strength, $k_2 \in -20, -10, 0, 10, 20$. Specifically, panels (a–c) depict $k_2 = -20$, (d–f) $k_2 = -10$, (g–i) $k_2 = 0$, (j–l) $k_2 = 10$, and (m–o) $k_2 = 20$. The figure highlights how varying higher-order coupling and noise strength jointly modulate the onset and extent of synchronization within the frustrated oscillator ensemble.

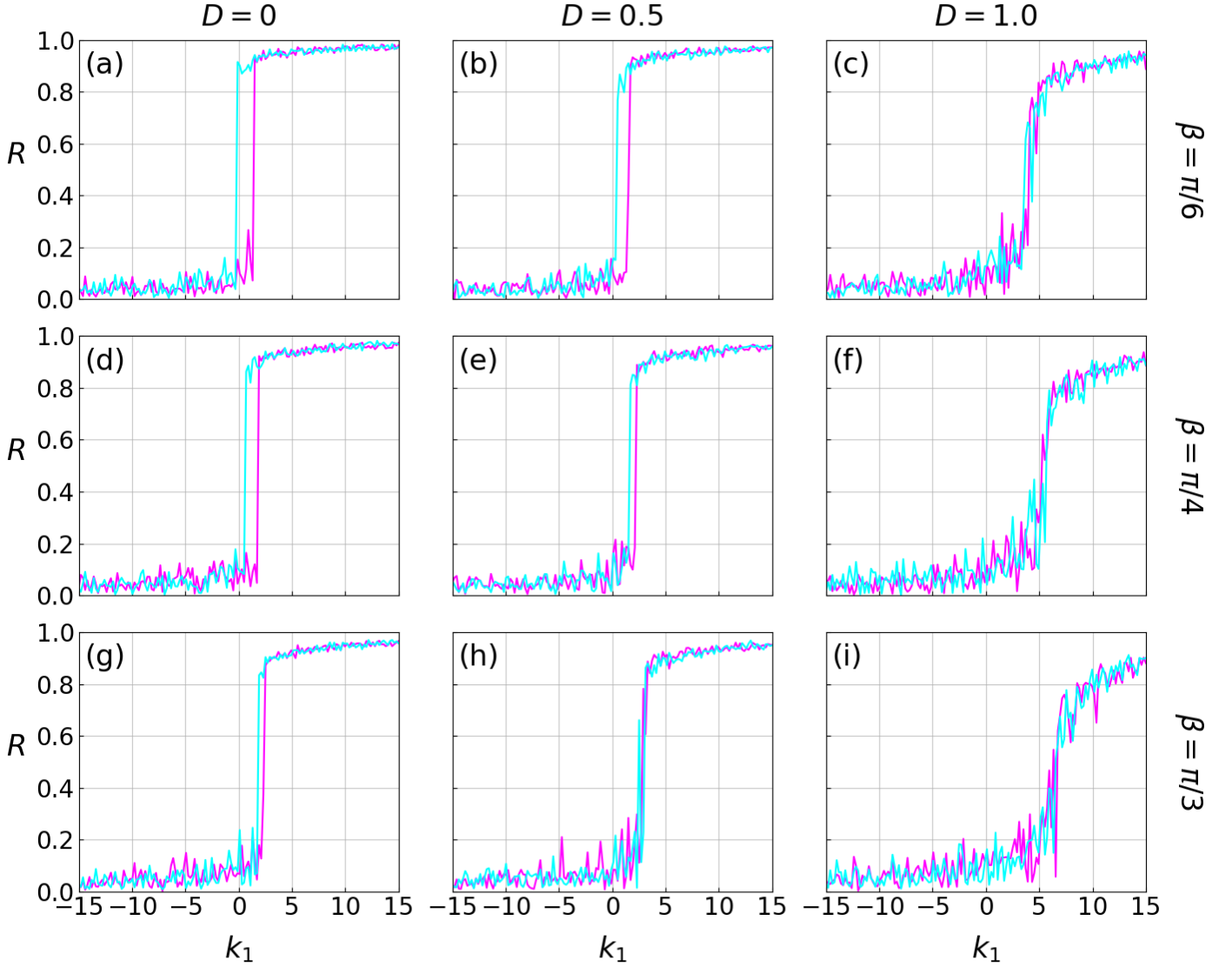


FIG. 3. Variation of the order parameter R as a function of the pairwise coupling strength k_1 for forward sweep (magenta color) and backward sweep (cyan color) simulations, at a fixed higher-order interaction strength $k_2 = 10$ for a system of $N = 100$ oscillators. Each column corresponds to a different noise strength: panels (a–g) correspond to $D = 0$, panels (b–h) are for the case when $D = 0.5$, and panels (c–i) correspond to $D = 1.0$; each row corresponds to a different phase-lag value: panels (a–c) for $\beta = \pi/6$, panels (d–f) for $\beta = \pi/4$, and panels (g–i) for $\beta = \pi/3$. The natural frequencies ω_i are drawn from a Lorentzian distribution with $\omega_0 = 0$ and width $\Delta = 0.5$. The initial condition is an equally populated bi-cluster state in which half of the oscillators have phase $\phi = 0$ and the remaining half of the oscillators have phase $\phi = \pi$. The figure demonstrates that the width of the hysteresis loop decreases systematically with increasing phase lag β and noise strength D .

Here, $g(\Omega)$ is the Lorentzian frequency distribution, and ρ_n is the coefficient of the n -th term of the series. Using the Ott-Antonsen ansatz, $\rho_n(\Omega, t) = \alpha^n(\Omega, t)$. Substituting Eq. 6–Eq. 9 in Eq. 5, we obtain:

$$\dot{\alpha} = (i\omega - D)\alpha + \frac{1}{2}[He^{-i\beta} - H^*e^{i\beta}\alpha^2] \quad (10)$$

Since the natural frequency distribution of the system is Lorentzian, the OA manifold is analytic in the lower half of the complex plane. Using Cauchy's integral theorem, we get $\bar{z}_1 = \alpha(\omega_0 - i\Delta, t)$. Similarly, we can derive $\bar{z}_2 = \alpha^2(\omega_0 - i\Delta, t) = \bar{z}_1^2$. At the pole $\omega = (\omega_0 - i\Delta)$, Eq. 10 leads

to

$$z_1 = (i\omega_0 - \Delta) + \frac{1}{2}(k_1 + k_2|z_1|^2)[He^{-i\beta} - H^*e^{i\beta}|z_1|^2z_1] \quad (11)$$

where $H = k_1z_1 + k_2z_2\bar{z}_1$

Since $z_1 = r_1e^{i\psi_1}$, comparing the real and imaginary parts of both sides of Eq. 11, we get a closed form (amplitude equation in terms of r and dropping the subscript) of the dynamical equation as follows:

$$\dot{r} = -(D + \Delta)r + \frac{\cos\beta}{2}(k_1r + k_2r^3)(1 - r^2) \quad (12)$$

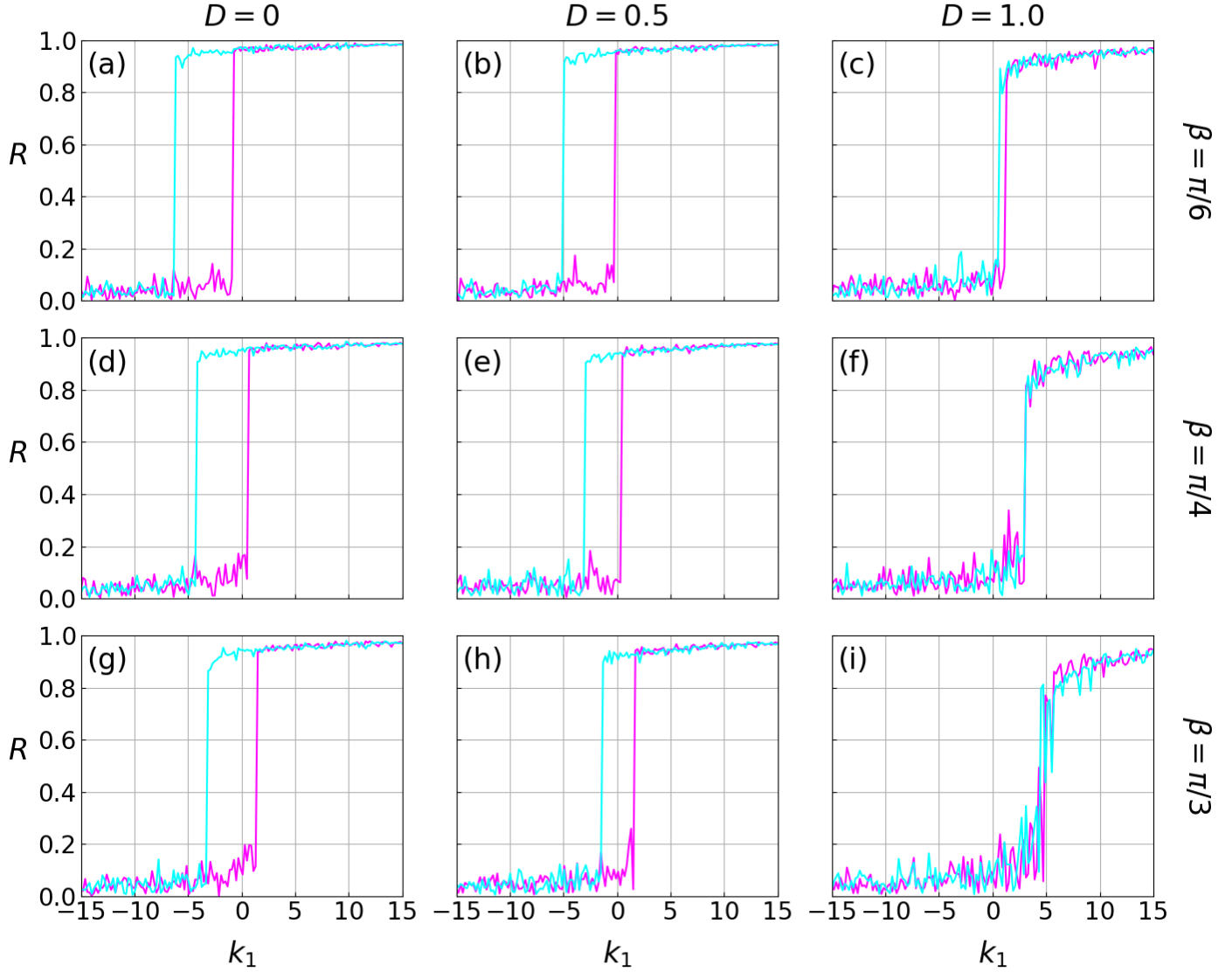


FIG. 4. Variation of the order parameter R as a function of the pairwise coupling strength k_1 for forward sweep (magenta color) and backward sweep (cyan color) simulations, at a fixed higher-order interaction strength $k_2 = 20$ for a system of $N = 100$ oscillators. Each column corresponds to a different noise strength: panels (a – g) correspond to $D = 0$, panels (b – h) are for the case when $D = 0.5$, and panels (c – i) correspond to $D = 1.0$; each row corresponds to a different phase-lag value: panels (a – c) for $\beta = \pi/6$, panels (d – f) for $\beta = \pi/4$, and panels (g – i) for $\beta = \pi/3$. The natural frequencies ω_i are drawn from a Lorentzian distribution with $\omega_0 = 0$ and a width $\Delta = 0.5$. The initial condition is an equally populated bi-cluster state in which half of the oscillators have phase $\phi = 0$, and the remaining half of the oscillators have phase $\phi = \pi$. The figure demonstrates that the width of the hysteresis loop decreases systematically with increasing phase lag β and noise strength D .

And the corresponding phase equation of the system can be written as:

$$\dot{\psi} = \omega_0 - \frac{\sin \beta}{2} (1 + r^2) (k_1 + k_2 r^2) \quad (13)$$

In case of no noise, Eq. 12 reduces to the theoretical calculation done in [46], thereby showing consistency with the existence theory.

In Fig. 5, we compare the theoretical amplitude obtained by simulating Eq. 12 with the numerical order parameter computed from Eq. 3, using the phases θ_i obtained from simulations of Eq. 1.

To further understand the bistability phenomenon in the network, we analyze the reduced dynamics (Eq. 12), identifying the fixed points and their stability, as well as bifurcations.

Fixed points: The solutions of Eq. 12 are obtained by setting $\dot{r} = 0$. One of the trivial solutions is $r^* = 0$, while the other solutions are obtained by solving Eq. 14.

$$-(\Delta + D) + \frac{\cos \beta}{2} (k_1 + k_2 r^2) (1 - r^2) = 0 \quad (14)$$

We obtain the following four nontrivial fixed points:

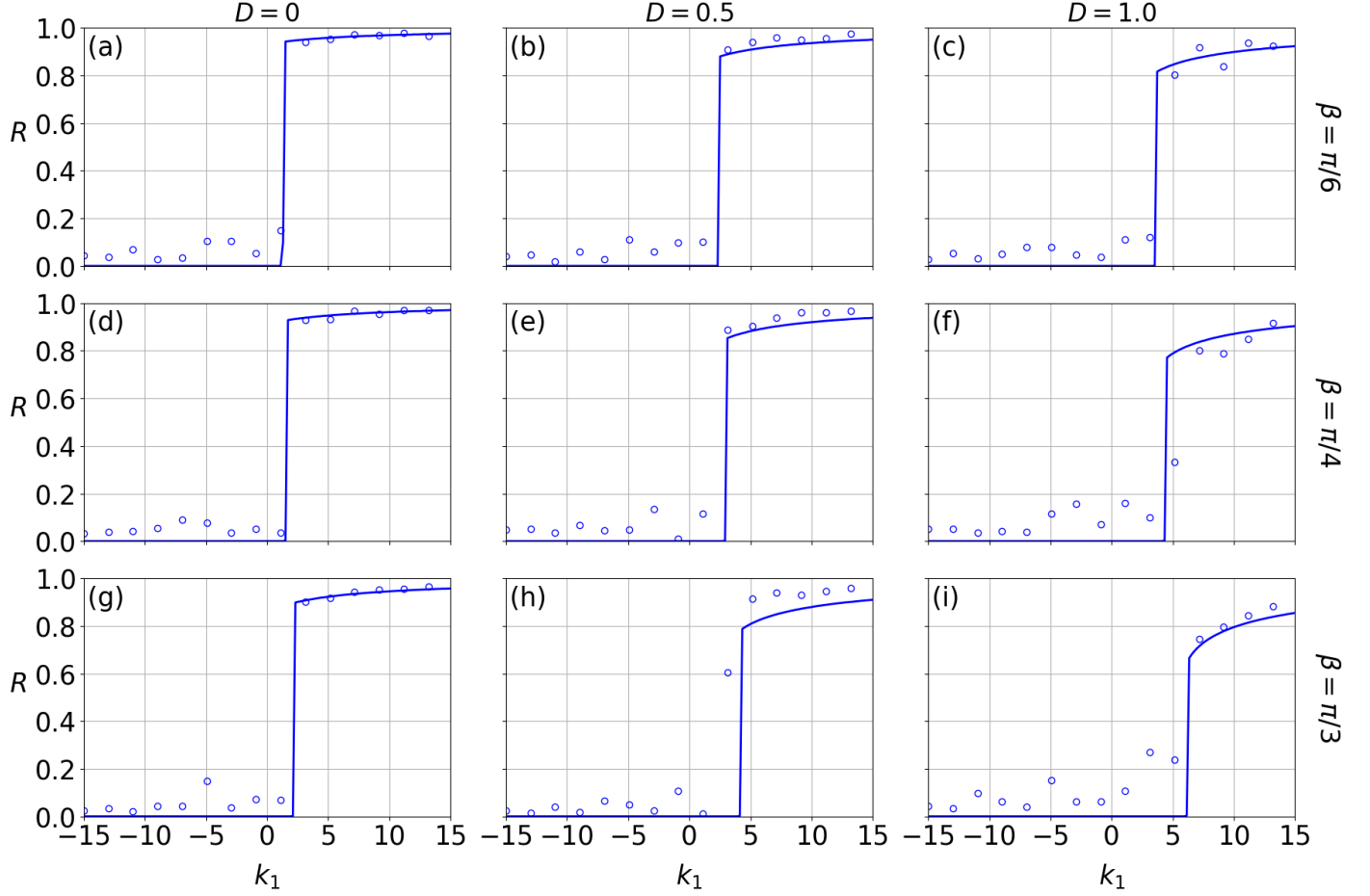


FIG. 5. Comparison of theoretical and numerical order parameters R as a function of the pairwise interaction strength k_1 for $N = 100$ coupled stochastic SK oscillators for a fixed higher-order (2-simplex) interaction strength $k_2 = 10$. Here, $\omega_0 = 0$ and $\Delta = 0.5$. The theoretical value of R (blue solid line) is obtained by solving Eq. (12), while the numerical values (blue circles) are computed by integrating Eq. (1). The first, second, and third columns correspond to noise strengths $D = 0, 0.5$, and 1 , respectively, whereas the rows correspond to phase-lag values $\beta = \pi/6, \pi/4$, and $\pi/3$. Panels (a–c) represent $\beta = \pi/6$, (d–f) correspond to $\beta = \pi/4$, and (g–i) to $\beta = \pi/3$. The results demonstrate good agreement between the theoretical predictions and numerical simulations across all parameter regimes.

$$r_{\pm}^* = \pm \sqrt{\frac{(k_2 - k_1) \pm \sqrt{(k_2 - k_1)^2 + 4k_2(k_1 - A)}}{2k_2}} \quad (15)$$

where $A = 2(\Delta + D)/\cos\beta$. The detailed steps for finding these fixed points are given in the supplementary information material (please refer to Sec. 2 of the supplementary material).

Since $r \in [0, 1]$, the only positive solution is physically relevant. Moreover, as we seek positive real solutions, the discriminant of Eq. 15 must be non-negative. Thus, we find only two physically relevant non-zero fixed points, which are the following:

$$r^* = \sqrt{\frac{(k_2 - k_1) \pm \sqrt{(k_2 - k_1)^2 + 4k_2(k_1 - A)}}{2k_2}} \quad (16)$$

Stability of fixed points: From the linear stability analysis, we find that $r^* = 0$ is always stable for $\cos\beta = 0$ (and

$\cos\beta > 0$). Similarly, it will be stable if $k_1 < \frac{2(\Delta+D)}{\cos\beta}$ (and $\cos\beta < 0$). And it will be stable if $k_1 > \frac{2(\Delta+D)}{\cos\beta}$. Linear stability analysis of the two physically relevant fixed points, the larger and small-amplitude solutions (cf. Eq. 16), shows that the large-amplitude fixed point r^* is stable, whereas the small-amplitude fixed point is unstable.

Bifurcation: As shown in Eq. 12, the reduced amplitude equation may take the normal form of either a subcritical or a supercritical pitchfork bifurcation depending on the signs of the coefficients of r^3 and r^5 (please refer to supplementary Sec. 2 for complete derivation). The figures, S1-S6 (please refer to the supplementary material Sec. 4), present a clear picture of subcritical and supercritical pitchfork bifurcations, depending on the parameter values. Further, we find critical points of the bifurcations. When the parameter k_1 is varied in the forward direction, the bifurcation point at which the trivial solution $r^* = 0$ loses stability is $k_{1c} = \frac{2(\Delta+D)}{\cos\beta}$. This transition marks the loss of stability of the trivial state and the emergence of the

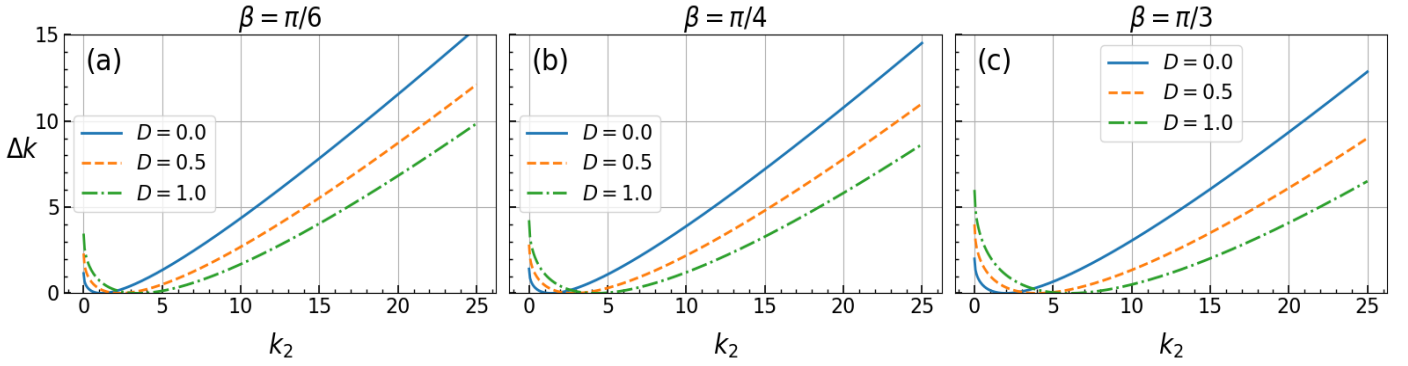


FIG. 6. The variation of the hysteresis width (Δk) vs. the strength of higher-order interaction (k_2) at different noise strengths $D = 0.0, 0.5, 1.0$. Panel (a,b,c) are for the phase lag values $\beta = \pi/6, \beta = \pi/4$, and $\beta = \pi/3$ respectively.

stable nontrivial state. In the backward direction, the two nontrivial fixed points (one stable and one unstable) collide at $r^* = \sqrt{\frac{k_2 - k_1}{2k_2}}$, indicating a saddle-node bifurcation. The corresponding critical value is $k_1^{\text{SN}} = -k_2 + 2\sqrt{\frac{2k_2(\Delta + D)}{\cos \beta}}$. The hysteresis width is given by $\Delta k = |k_{1c} - k_1^{\text{SN}}|$.

As we can clearly see from Fig. 6 that the hysteresis width depends on the frustration parameter β , the noise intensity D , and largely on the higher-order coupling strength k_2 . This behavior is fully consistent with our theoretical predictions; for example, for fixed values of the other parameters, increasing k_2 decreases the saddle-node point k_1^{SN} , while the forward critical point k_{1c} remains unchanged because it does not depend on k_2 . Consequently, the separation between k_{1c} and k_1^{SN} increases, resulting in a broader bistable region and an earlier onset of synchronization. This is also consistent with the numerical results we obtain for the N coupled systems. To further understand how noise affects the stability of this multistable regime, we analyze the system using Kramers' escape rate.

Kramers' escape rate: Kramers' escape rate describes the noise-induced transition probability between coexisting stable states in a bistable potential. In a system with two stable fixed points separated by an unstable barrier, small noise perturbs the dynamics within each basin of attraction, while sufficiently strong fluctuations allow the state variable to cross the potential barrier and switch to the other stable state. Kramers' theory quantifies the mean escape time from the bottom of the well (stable point) to the top of the well (unstable point) as $\Gamma \propto e^{(-\Delta V(k_1, k_2)/D)}$ (please refer to the supplementary Sec. 3 for the complete derivation), where ΔV is the height of the potential barrier and D is the noise intensity. When D increases at fixed β , the escape rate of the system from one stable state to another state decreases. This implies that the system takes a shorter time to switch from the stable to the unstable state, leading to a reduction in the hysteresis width (Fig. 3a, Fig. 3b, Fig. 3c). However, the barrier potential height, ΔV , depends positively on the strength of the higher-order interactions k_2 (please refer to Sec. 3 of the supplementary material for the complete derivation), so when k_2 is large, the system resists the stochastic forcing, spending more time in the

metastable state, and exhibits a broader hysteresis width (Fig. 4a, Fig. 4b, Fig. 4c, for $k_2 = 20$). For a fixed noise strength, D , increasing the phase lag from $\beta = \pi/6$ to $\beta = \pi/3$ (Fig. 4c, Fig. 4f, Fig. 4i) reduces the effective coupling ($\cos \beta$ factor in Eq. 12), which in turn decreases the order-parameter amplitudes r_1, r_2 , and as a result the barrier height ΔV , according to Kramers' escape rate formula, a smaller barrier yields a larger escape rate and a shorter metastable life, and this is consistent with our numerical results.

IV. CONCLUSION

We investigated the combined influence of phase frustration, noise, and higher-order interactions on synchronization in a globally coupled Kuramoto–Sakaguchi network. Our numerical results reveal that synchronization arises from a nontrivial interplay among these three mechanisms. Under strong internal phase frustration, coherence emerges only when both coupling strengths are repulsive, although sufficiently large negative 2 – *simplex* coupling can induce synchronization even for small positive values of 1 – *simplex* interaction strength. When phase frustration is weak, synchronization is favored when both interaction strengths are positive; if one coupling becomes slightly negative, the other must be sufficiently strong to maintain coherence. Thus, in general, weak frustration combined with mutually reinforcing coupling promotes synchronization, whereas strong frustration favors coherence under repulsive coupling.

Further, we observed a range of dynamical phenomena, including first- and second-order phase transitions, hysteresis, and bistability, where synchronization and desynchronization coexist. Increasing noise intensity suppresses coherence but also smooths the transition from desynchronization to synchronization. Multi-stability is supported by low frustration, weak noise, and strong higher-order coupling. Higher-order interactions widen the multistable region by shifting the backward saddle-node point without affecting the forward critical point. To explain these observations, we applied the Ott–Antonsen reduction to

derive a low-dimensional amplitude equation that helps determine the steady states, their stability, bifurcation types, forward and backward critical transition points, and hysteresis width, thereby verifying our observed numerical results. Furthermore, by analyzing Kramers' escape rate, we provided a mechanistic explanation for how noise destabilizes the coexistence of synchronized and desynchronized states, thereby shrinking or eliminating the bistable region depending on parameter values.

Overall, our study establishes a unified framework for understanding synchronization in frustrated, noisy, higher-order networks. Our findings demonstrate that higher-order interactions can stabilize coherence even in the presence of noise and internal phase lag, offering new insights into biological, physical, and engineered systems where collective dynamics emerge from complex multi-scale interactions shaped by frustration and stochasticity. This work opens avenues for future studies on spatially extended systems, heterogeneous networks, time-delayed interactions, and adaptive simplicial structures, where the interplay between noise and higher-order coupling may generate even more diverse dynamical behaviors.

DATA AVAILABILITY STATEMENT

Data sharing is not applicable to this article, as no new data were created or analyzed in this study.

ACKNOWLEDGMENTS

We wish to acknowledge Prof. Hiroshi Kori (*University of Tokyo, Japan*) for fruitful discussions. CM acknowledges support from the Anusandhan National Research Foundation (ANRF) India (Grant Numbers SRG/2023/001846 and EEQ/2023/001080) and the INSPIRE-Faculty Grant (No. IFA19-PH248).

SUPPLEMENTARY MATERIAL REFERENCE

Detailed derivations and intermediate steps of the analytical analysis are provided in the supplementary material.

-
- [1] S. H. Strogatz, From kuramoto to crawford: exploring the onset of synchronization in populations of coupled oscillators, *Physica D: Nonlinear Phenomena* **143**, 1 (2000).
 - [2] J. Buck, Synchronous rhythmic flashing of fireflies. ii., *The Quarterly review of biology* **63**, 265 (1988).
 - [3] P. D. Rungta, A. Choudhary, C. Meena, and S. Sinha, Are network properties consistent indicators of synchronization?, *Europhysics Letters* **117**, 20003 (2017).
 - [4] S. Acharyya, P. Pradhan, and C. Meena, Master stability functions in complex networks, *arXiv preprint arXiv:2412.19163* (2024).
 - [5] A. Ghosh, Measure synchronization in interacting hamiltonian systems: A brief review, *Chaos, Solitons & Fractals* **177**, 114237 (2023).
 - [6] M. Mehrabbeik, A. Ahmadi, F. Bakouie, A. H. Jafari, S. Jafari, and D. Ghosh, The impact of higher-order interactions on the synchronization of hindmarsh-rose neuron maps under different coupling functions, *Mathematics* **11**, 2811 (2023).
 - [7] Z. Wang, M. Chen, X. Xi, H. Tian, and R. Yang, Multi-chimera states in a higher order network of fitzhugh–nagumo oscillators, *The European Physical Journal Special Topics* **233**, 779 (2024).
 - [8] C. Meena, S. Kumari, A. Sharma, and S. Sinha, Effect of heterogeneity in a model of el nino southern oscillations, *Chaos, Solitons and Fractals* **104**, 668 (2017).
 - [9] H. Taher, S. Olmi, and E. Schöll, Enhancing power grid synchronization and stability through time-delayed feedback control, *Phys. Rev. E* **100**, 062306 (2019).
 - [10] M.-C. Ho, Y.-C. Hung, and C.-H. Chou, Phase and anti-phase synchronization of two chaotic systems by using active control, *Physics Letters A* **296**, 43 (2002).
 - [11] V. Anishchenko, O. Sosnovtseva, A. Kopejkin, D. Matujshkin, and A. Klimshin, Synchronization effects in networks of stochastic bistable oscillators, *Mathematics and Computers in Simulation* **58**, 469 (2002), *chaos Synchronization and Control*.
 - [12] R. Berner, E. Scholl, and S. Yanchuk, Multiclusters in networks of adaptively coupled phase oscillators, *SIAM Journal on Applied Dynamical Systems* **18**, 2227 (2019).
 - [13] Y. Zhang and J. Sun, Chaotic synchronization and anti-synchronization based on suitable separation, *Physics Letters A* **330**, 442 (2004).
 - [14] C. Meena, K. Murali, and S. Sinha, Chimera states in star networks, *International Journal of Bifurcation and Chaos* **26**, 1630023 (2016).
 - [15] A. T. Winfree, *The Geometry of Biological Time* (Springer Berlin, Heidelberg, 1980).
 - [16] Y. Kuramoto, *Chemical Oscillations, Waves, and Turbulence* (Springer, New York, 1984).
 - [17] S. H. Strogatz, From kuramoto to crawford: exploring the onset of synchronization in populations of coupled oscillators, *Physica D: Nonlinear Phenomena* **143**, 1 (2000).
 - [18] J. A. Acebrón, L. L. Bonilla, C. J. Pérez Vicente, F. Ritort, and R. Spigler, The kuramoto model: A simple paradigm for synchronization phenomena, *Rev. Mod. Phys.* **77**, 137 (2005).
 - [19] J. W. Swift, S. H. Strogatz, and K. Wiesenfeld, Averaging of globally coupled oscillators, *Physica D: Nonlinear Phenomena* **55**, 239 (1992).
 - [20] K. Wiesenfeld, P. Colet, and S. H. Strogatz, Synchronization transitions in a disordered josephson series array, *Phys. Rev. Lett.* **76**, 404 (1996).
 - [21] M. Ramasamy, S. Devarajan, S. Kumarasamy, and K. Rajagopal, Effect of higher-order interactions on synchronization of neuron models with electromagnetic induction, *Applied Mathematics and Computation* **434**, 127447 (2022).
 - [22] A. Farrera-Megchun, P. Padilla-Longoria, G. J. E. Santos, J. Espinal-Enríquez, and R. Bernal-Jaquez, Explosive synchronization driven by repulsive higher-order interactions in coupled neurons, *Chaos, Solitons & Fractals* **196**, 116368 (2025).
 - [23] T. J. Walker, Acoustic synchrony: two mechanisms in the snowy tree cricket, *Science* **166**, 891 (1969).
 - [24] S. Strogatz, D. Abrams, A. McRobie, B. Eckhardt, and E. Ott, Crowd synchrony on the millennium bridge, *Nature* **438**, 43 (2005).
 - [25] B. Eckhardt, E. Ott, S. H. Strogatz, D. M. Abrams, and A. McRobie, Modeling walker synchronization on the millennium bridge, *Phys. Rev. E* **75**, 021110 (2007).
 - [26] E. Ott and T. M. Antonsen, Low dimensional behavior of large systems of globally coupled oscillators, *Chaos: An Interdisciplinary Journal of Nonlinear Science* **18** (2008).
 - [27] J. D. Crawford, Amplitude expansions for instabilities in populations of globally-coupled oscillators, *Journal of statistical physics* **74**, 1047 (1994).
 - [28] E. A. Martens, E. Barreto, S. H. Strogatz, E. Ott, P. So, and T. M.

- Antonsen, Exact results for the kuramoto model with a bimodal frequency distribution, *Phys. Rev. E* **79**, 026204 (2009).
- [29] Y. Moreno and A. F. Pacheco, Synchronization of kuramoto oscillators in scale-free networks, *Europhysics Letters* **68**, 603 (2004).
- [30] H. Daido, Multibranch entrainment and scaling in large populations of coupled oscillators, *Physical review letters* **77**, 1406 (1996).
- [31] F. Battiston, G. Cencetti, I. Iacopini, V. Latora, M. Lucas, A. Patania, J.-G. Young, and G. Petri, Networks beyond pairwise interactions: Structure and dynamics, *Physics reports* **874**, 1 (2020).
- [32] S. Boccaletti, P. De Lellis, C. Del Genio, K. Alfaro-Bittner, R. Criado, S. Jalan, and M. Romance, The structure and dynamics of networks with higher order interactions, *Physics Reports* **1018**, 1 (2023).
- [33] P. S. Skardal and A. Arenas, Higher order interactions in complex networks of phase oscillators promote abrupt synchronization switching, *Communications Physics* **3**, 218 (2020).
- [34] Q. Dai and H. Kori, Higher-order synchronization and multistability in higher-order kuramoto phase oscillators, *Nonlinear Dynamics* **113**, 21801 (2025).
- [35] M. Brede and A. C. Kalloniatis, Frustration tuning and perfect phase synchronization in the kuramoto-sakaguchi model, *Phys. Rev. E* **93**, 062315 (2016).
- [36] Y. Kuramoto and D. Battogtokh, Coexistence of coherence and incoherence in nonlocally coupled phase oscillators, *arXiv preprint cond-mat/0210694* (2002).
- [37] M. Rohden, A. Sorge, M. Timme, and D. Witthaut, Self-organized synchronization in decentralized power grids, *Phys. Rev. Lett.* **109**, 064101 (2012).
- [38] F. Dörfler and F. Bullo, Synchronization and transient stability in power networks and nonuniform kuramoto oscillators, *SIAM Journal on Control and Optimization* **50**, 1616 (2012), <https://doi.org/10.1137/110851584>.
- [39] D. S. Goldobin and A. Pikovsky, Synchronization and desynchronization of self-sustained oscillators by common noise, *Physical Review E—Statistical, Nonlinear, and Soft Matter Physics* **71**, 045201 (2005).
- [40] A. Campa and S. Gupta, Synchronization in a system of kuramoto oscillators with distributed gaussian noise, *Phys. Rev. E* **108**, 064124 (2023).
- [41] J. Vukadinovic, Traveling waves in the mckean-vlasov equation under sakaguchi-kuramoto interaction with phase frustration, *arXiv preprint arXiv:2510.18059* (2025).
- [42] W. Yue, L. D. Smith, and G. A. Gottwald, Model reduction for the kuramoto-sakaguchi model: The importance of nonentrained rogue oscillators, *Phys. Rev. E* **101**, 062213 (2020).
- [43] P. S. Skardal, Low-dimensional dynamics of the kuramoto model with rational frequency distributions, *Phys. Rev. E* **98**, 022207 (2018).
- [44] A. Carballosa, A. P. Muñuzuri, S. Boccaletti, A. Torcini, and S. Olmi, Cluster states and pi-transition in the kuramoto model with higher order interactions, *Chaos, Solitons and Fractals* **177**, 114197 (2023).
- [45] A. Suman and S. Jalan, Finite-size effect in kuramoto oscillators with higher-order interactions, *Chaos: An Interdisciplinary Journal of Nonlinear Science* **34** (2024).
- [46] S. Dutta, A. Mondal, P. Kundu, P. Khanra, P. Pal, and C. Hens, Impact of phase lag on synchronization in frustrated kuramoto model with higher-order interactions, *Phys. Rev. E* **108**, 034208 (2023).